Journal of Materials Chemistry A

PAPER

View Article Online
View Journal | View Issue

Cite this: J. Mater. Chem. A, 2015, 3, 9989

Role of crystallinity of non-fullerene acceptors in bulk heterojunctions†

Jes B. Sherman,[a] Balaji Purushothaman,[b] Sean R. Parkin,[b] Chunki Kim,[a] Sam Collins,[a] John Anthony,[b] Thuc-Quyen Nguyen[a] and Michael L. Chabinyc*[c]

Received 13th February 2015
Accepted 25th March 2015

DOI: 10.1039/c5ta01206f

www.rsc.org/MaterialsA

Understanding the solid-state structure of the bulk heterojunction provides insight into how to improve the performance of nonfullerene acceptors in organic solar cells. We have characterized the self-assembly of three functionalized pentacene acceptors in single crystals, neat films and bulk heterojunctions formed by blending with a diketopyrrolopyrrole-based molecular donor. Atomic force microscopy, grazing incidence wide-angle X-ray scattering and optical spectroscopy indicate that the presence of the donor perturbs the packing and texture of acceptors with smaller substituents. The structural characterization explains the differences in performance among the three acceptors studied and suggests that, unlike fullerenes, disordered domains of molecular acceptors with planar molecular structure have inefficient electron transport in BHJ thin films.

Introduction

Organic photovoltaics (OPVs) are a class of thin film solar cells that can be fabricated by deposition from solvents using simple printing methods. The highest performance OPVs are bulk heterojunctions (BHJs), where an electron donating material and an electron accepting material are dissolved together in solution and then cast into a blended thin film.[1,2] BHJ solar cells with both small molecule and polymer donors with fullerene-based acceptors have been demonstrated with power conversion efficiencies approaching 10%.[3–5] Due to the relatively short exciton diffusion lengths in organic semiconductors (~10 nm), the length scale of phase separation of the donor and acceptor domains in efficient BHJs is ideally on the order of 20 nm. Because of this complex morphology, BHJs present an opportunity to exploit molecular self-assembly and to investigate the role of molecular packing within biphasic blends.

The formation of efficient BHJs relies on the nanoscale phase separation of the donor and acceptor upon casting. If the donor and acceptor crystallize readily, the phase separation process is additionally complicated by the kinetics of the growth of crystalline domains. Here, we study the role of crystallization of non-fullerene acceptors in BHJs using a series of silylethyne-substituted pentacenes as acceptors with a well-performing diketopyrrolopyrrole-based donor. Systematic investigation of alternative acceptors with a fixed donor is a necessary step in the development of design rules for molecular BHJ OPVs.[6,7] Our results demonstrate the critical role of molecular packing in thin films on the properties of small molecule BHJs.

Using molecular semiconductors instead of polymers in BHJ solar cells affords an opportunity to explore structure–property relationships with materials that are inherently monodisperse and can be purified by simple methods such as recrystallization.[8,9] Molecular materials can be deposited by solution casting or by vapor deposition, allowing both the donor and acceptor to be cast from solution or by a combination of solution and vapor deposition.[10–12] Many small molecules exhibit high optical extinction coefficients in thin films, up to 10^5 cm^{-1}, and have broad overlap with the solar spectrum.[13] Additionally, materials can behave as either donors or acceptors in BHJs by attaching substituents that donate or withdraw electrons from the aromatic core to tune their electronic levels.[11]

The acceptor in a BHJ has an important role in charge generation and also in setting the open circuit voltage (V_{oc}).[14,15] Because the molar ratio of donor to acceptor is generally near one in BHJs, it is desirable that the optical absorption of each are both strong and have complementary overlap with the solar spectrum. Fullerenes are the most widely used acceptors due to the ability to promote efficient charge generation and charge extraction despite their relatively poor optical absorption coefficient (relative to the donor). Non-fullerene acceptors have been demonstrated to form BHJs with reasonable power conversion efficiencies, but they are still below the performance of fullerene-based BHJs with the same donor.[6,7,14,16–21]

It is not well understood why non-fullerene acceptors underperform relative to their fullerenes using a common

[a]Department of Chemistry and Biochemistry, University of California Santa Barbara, Santa Barbara, CA 93106, USA

[b]Department of Chemistry, University of Kentucky, Lexington, KY 40506, USA

[c]Materials Department, University of California Santa Barbara, Santa Barbara, CA 93106, USA. E-mail: mchabinyc@engineering.ucsb.edu

† Electronic supplementary information (ESI) available: Synthetic procedures for the acceptors, processing conditions for solar cells, spectroscopic data, conductive AFM data, and details of GIWAXS experiments. See DOI: 10.1039/c5ta01206f

donor.[22] It is possible that the answer lies within the observed morphology of highly efficient fullerene-based BHJs. Fullerenes are disordered in BHJs, showing only broad X-ray scattering peaks even in the presence of a highly ordered donor.[23] The overlap of the molecular orbitals between two adjacent, nearly spherical fullerenes does not depend strongly on orientation. Charge transport is therefore tolerant of molecular disorder. In contrast, most non-fullerene acceptors have a relatively planar structure, dictating that the strongest electronic coupling (and thus efficient electron transport) between molecules occurs when they are oriented co-facially.[24] As a consequence, these π–π interactions will promote the assembly of crystalline domains within a blend film. For example, a recent study using electron-deficient pentacene acceptors with P3HT as the donor showed large-scale crystal growth through the film for acceptors that pack with strong cofacial π–π interactions, whereas acceptors with sandwich herringbone crystal packing (containing fewer cofacial interactions) formed blend films without obvious large-scale phase separation, and exhibited higher power conversion efficiency.[25,26] With this in mind, we expect that the molecular packing of small acceptors (that is, the interactions between molecules in the solid state) has significant influence on their thin film morphology and their resulting optoelectronic behavior.[26,27]

We present here a study of the molecular ordering of silylethyne-substituted pentacenes with a common molecular donor in BHJs. These materials are particularly useful for the examination of structure–property relationships in small molecule BHJs because their crystal packing can be tuned relatively independently of their electronic transport levels simply by altering the peripheral trialkylsilyl substituent.[28] We focus on the octafluoropentacene derivatives shown in Fig. 1 because fluorination has been shown to yield highly stable materials with good electron transport properties.[29,30] The ionization energy and electron affinity (HOMO and LUMO energy levels) of these compounds (Table 1) are suitable for use as acceptors with diketopyrrolopyrrole-based donors, and we expected high open circuit potentials (~1.0 V) to result from the pairing. Diketopyrrolopyrroles have high optical extinction coefficients, on the order of 10^4 M^{-1} cm^{-1} in solution, and BHJs with modest power conversion efficiencies have been made with them

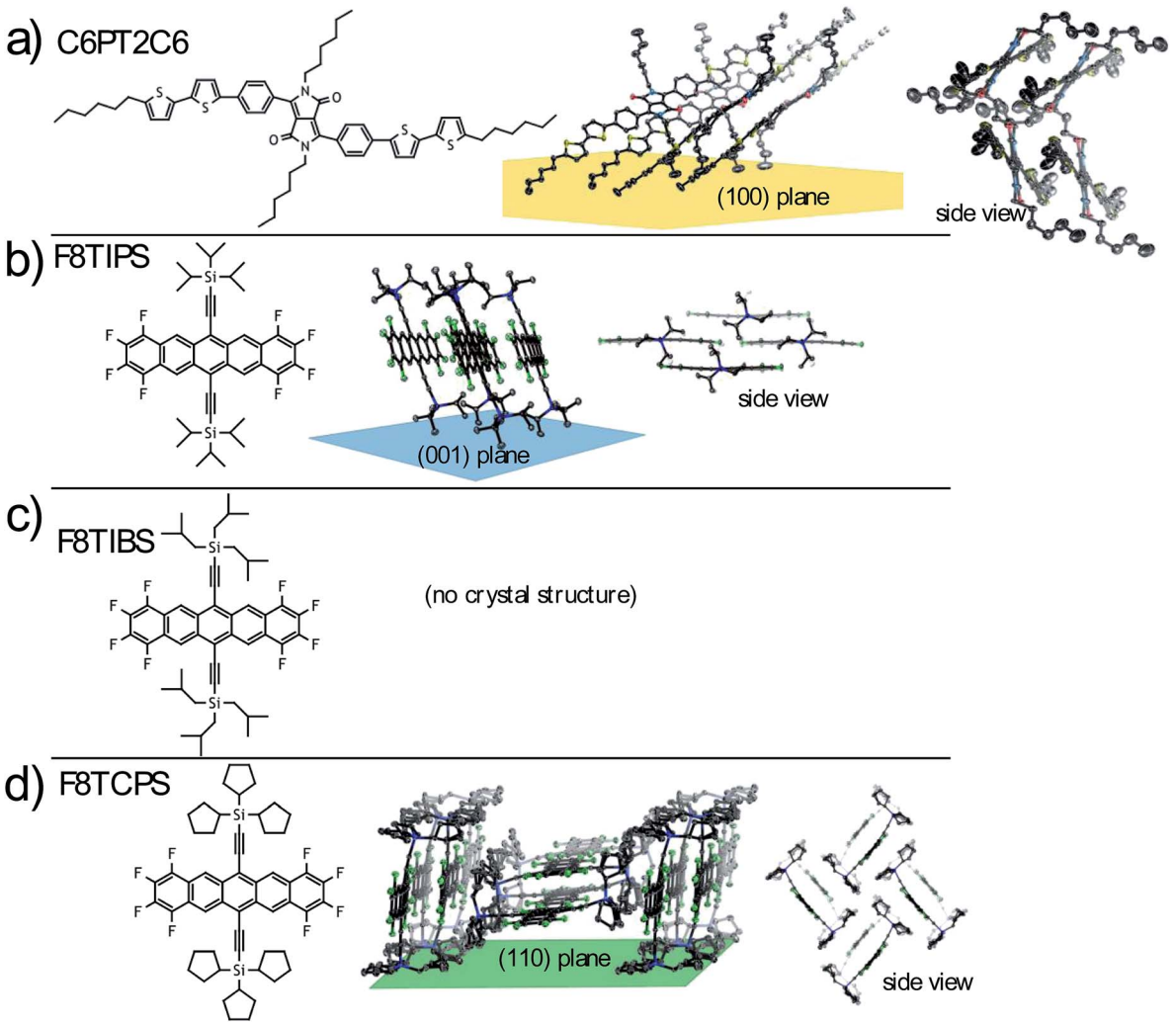

Fig. 1 Chemical structures and diagrams of crystal packing of the donor (C6PT2C6) and the acceptors (F8TIPS, F8TIBS, and F8TCPS).

Table 1 Ionization energies (IE) and estimated electron affinity (EA) of the donor (C6PT2C6) and the acceptors (F8TIPS, F8TIBS, F8TCPS). The IEs were determined by UPS (on thin films); the EAs were estimated using the optical bandgap from the absorption edge of thin film UV/Vis spectra. Data for C6PT2C6 taken from ref. 26

	C6PT2C6	F8TIPS	F8TIBS	F8TCPS
IE (eV)	5.16	5.51	5.59	5.71
EA (eV)	3.32	3.56	3.61	3.71

with fullerene acceptors.[31,32] Using a combination of X-ray scattering, conducting probe atomic force microscopy, optical characterization, and device measurements, we examine how this series of non-fullerene acceptors and molecular donor crystallize and phase separate in BHJ films.[33] Although the resulting power conversion efficiencies of the cells are low, our results reveal how crystallization affects the morphology and performance of these small molecule BHJs.

Results and discussion

Single crystal structures of pentacene-based acceptors and diketopyrrolopyrrole-based donor

In thin films of small molecule BHJ blends, both the donor and the acceptor may crystallize, leading to a complex evolution of the phase separated morphology during deposition or during post treatments.[34] Because many organic semiconductors exhibit thin film polymorphs or form co-crystals, it is also of interest to develop a better understanding of how the solid-state organization is perturbed by the addition of a second component a blended thin film.[35–38] In many cases, single crystal structures are not available, complicating quantitative analysis of X-ray scattering data from thin films.[39]

The single crystal structures of the donor and acceptors provide a means to determine if ordered domains in thin films have the same packing structure as the bulk crystals. The single crystal structures of the donor, C6PT2C6, and one of the acceptors F8TIPS were previously determined. The structure of F8TCPS was solved here (CCDC 1034523). The crystal structure of F8TIBS could not be determined because high quality single crystals could not be grown. As shown in Fig. 1, the donor material in this study, C6PT2C6, packs in a gamma-motif with close contacts between adjacent molecules within a stack.[26,31] As reported previously, F8-TIPS packs in a similar fashion to TIPS pentacene; that is, close cofacial stacking between aromatic cores.[40,41] F8-TCPS packs in a "sandwich herringbone" motif.[26] This packing motif in pentacene acceptors has consistently produced the highest photocurrents in OPV devices using polymer donors.[25,42] Using these single crystal structures, we quantified the molecular orientation in thin films by examining the texture of the crystallites (*vide infra*).

Characteristics of bulk heterojunction solar cells

In order to relate the thin film structure to the current–voltage characteristics of solar cells, we fabricated BHJ solar cells and optimized the annealing temperatures and blend ratios through empirical testing (details in ESI†). We have used a common donor molecule, C6PT2C6, for all the BHJs. This donor material exhibits a moderate hole mobility ($\sim 2 \times 10^{-3}$ cm^2 V s^{-1}) in organic thin film transistors and has been successfully used as a donor in OPV devices with fullerene acceptors.[43] BHJ films were spun-cast and processed according to procedures listed in the ESI.† UV/Vis spectra of the BHJ films (Fig. 2) show that they absorb light from about 275 nm up to about 700 nm. The long wavelength absorption edge is set by the acceptor rather than the donor, in contrast to many fullerene-based BHJs where the donor has the lowest optical edge.[44] The current–voltage (J–V) response of the solar cells under AM1.5 simulated solar illumination are shown in Fig. 3, and their characteristics including the short circuit current, J_{sc}, open circuit voltage, V_{oc}, fill factor, FF, and power conversion efficiency are summarized in Table 2. While the open circuit voltage was near 1.0 V for all the devices, the absolute power conversion efficiencies were low (<1%) due to the J_{sc}. These results with TIPS-pentacene acceptors can be compared to C6PT2C6:PC$_{71}$BM solar cells that have V_{oc} of 0.90, J_{sc} 7.9 mA cm^{-2} and FF = 0.49.[45] Clearly the largest

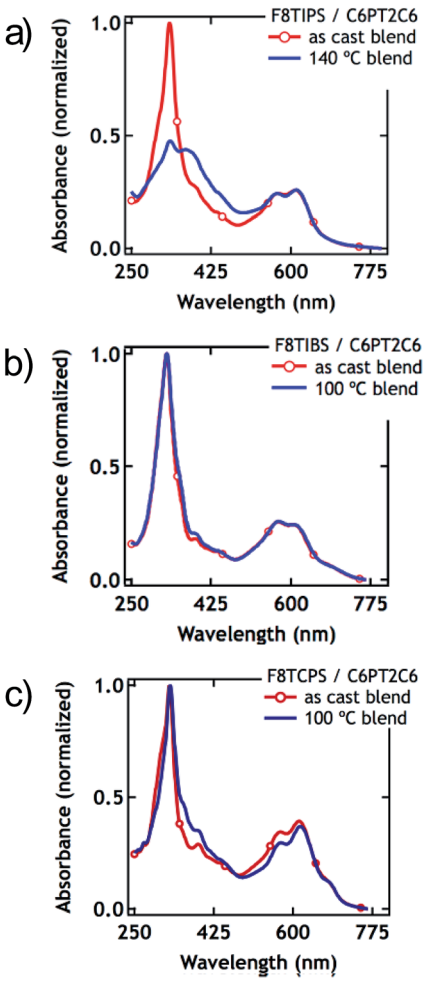

Fig. 2 Thin film absorption spectra on of the BHJs before and after annealing on quartz. The BHJ films were spun-cast at 2000 RPM/60 s from 1.5% (w/v) chloroform solutions.

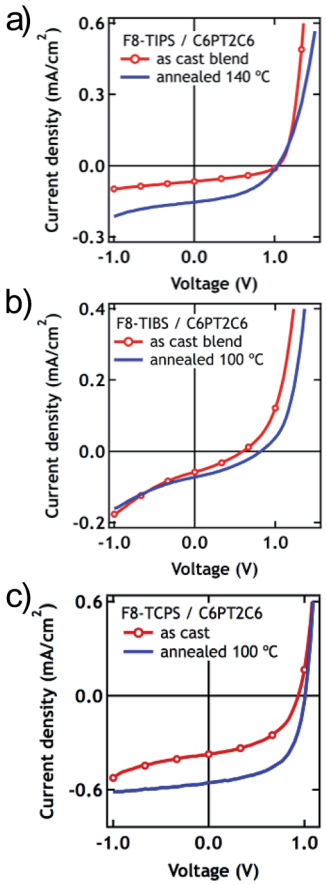

Fig. 3 Current–voltage characteristics of the BHJs using (a) F8-TIPS, (b) F8-TIBS, and (c) F8-TCPS. All films were spun-cast at 2000 RPM for 60 s from 1.5% w/v solutions in chloroform; blend ratio 1 : 1 by weight. Information about the device structure can be found in the ESI† and the solar cell characteristics are summarized in Table 2.

difference is the short circuit current suggesting inefficient charge generation or extraction in the non-fullerene cells here.

Photoluminescence (PL) quenching data suggests that charge extraction before recombination is a major cause of the low PCE. PL data was obtained by excitation at 520 nm, which dominantly excites the donor, C6PT2C6. TIPS-pentacene derivatives are known to have a very low PL yield, so we did not pursue PL studies by excitation of the acceptor.[46] The PL data (Fig. 4) shows emission from C6PT2C6 as expected and the quenching yield was relatively high (>50%) for the BHJ blends over a range of annealing temperatures. Because of the overlap of the emission of C6PT2C6 and the absorption of TIPS-pentacene acceptors, we expect that energy transfer from the donor to the acceptor will occur and aid in bringing excitons to the donor–acceptor interface over a longer range than just exciton diffusion.[44] The very low PL yield of the acceptors makes it difficult to study this process in detail. The PL data from excitation of the donor suggests clearly that the excitons are quenched (Fig. 4), but any charges that are generated are not extracted efficiently, *i.e.* they recombine. We therefore sought to understand the origin of the low PCE despite relatively good PL quenching by studying the morphology of these BHJs.

Molecular ordering in thin films

In order to probe molecular packing and film morphology within the BHJ, grazing incidence wide angle X-ray scattering (GIWAXS) was used to determine if the donors and acceptors crystallized upon spin casting or after thermal treatment in both neat and blend films. A synchrotron source was used because high flux is necessary in structural investigations of thin films of materials with structural disorder. Additionally, the use of 2D detection allowed a large area of reciprocal space to be measured, simultaneously minimizing damage done to the sample by X-ray exposure. First we outline how the donor orders in neat films, then we describe the structural changes in the donor and the acceptors when blended into BHJs.

Thin films of donor C6PT2C6. GIWAXS from as-cast thin films (roughly 100 nm thick) of C6PT2C6 reveals that the molecules crystallize with essentially the same unit cell as the bulk crystal structure (Fig. 5). The scattering peaks of the bulk structure were compared to the 2D GIWAXS data using Sim-Diffraction, a code developed to simulate the thin film diffraction pattern for a given crystal structure and film texture.[47] The overlay of the predicted and experimental data does not show peaks along q_z because this data is not accessible using the experimental geometry, and the simulated data shown have been calculated assuming all crystallites are perfectly oriented with respect to the substrate. Small differences in the unit cell parameters of C6PT2C6 are observed in thin films and we attributed these to the different data collection temperatures

Table 2 Average characteristics along with standard deviation of BHJ solar cells of C6PT2C6 with the acceptors, listed at top, under various processing conditions (as cast, thermally annealed). Hole and electron mobilities were determined from space charge limited current measurements of single-carrier diodes (as described in ESI)

	F8TIPS		F8TIBS		F8TCPS	
Condition	As cast	140 °C	As cast	100 °C	As cast	100 °C
V_{oc} (V)	0.88 ± 0.22	0.96 ± 0.11	0.47 ± 0.37	0.77 ± 0.27	0.80 ± 0.12	0.91 ± 0.13
J_{sc} (mA cm^{-2})	0.10 ± 0.02	0.15 ± 0.01	0.05 ± 0.01	0.06 ± 0.01	0.60 ± 0.13	0.66 ± 0.10
FF	0.37 ± 0.08	0.41 ± 0.05	0.26 ± 0.10	0.34 ± 0.05	0.43 ± 0.06	0.45 ± 0.09
PCE (%)	0.03 ± 0.02	0.06 ± 0.01	0.01 ± 0.01	0.02 ± 0.01	0.21 ± 0.07	0.28 ± 0.10
Devices tested	22	5	29	12	33	55
μ_h (cm^2 V s^{-1})	2.0×10^{-5}	1.2×10^{-5}	1.1×10^{-5}	1.5×10^{-5}	5.5×10^{-6}	1.5×10^{-5}
μ_e (cm^2 V s^{-1})	3.9×10^{-5}	1.4×10^{-5}	1.4×10^{-5}	1.6×10^{-5}	1.5×10^{-5}	1.5×10^{-4}

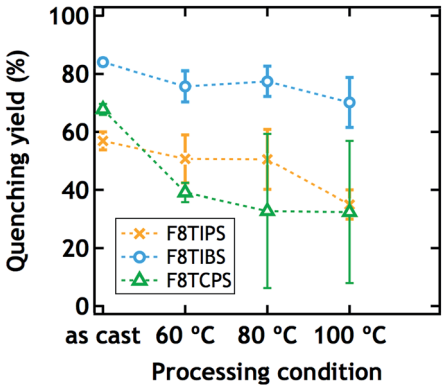

Fig. 4 Photoluminescence (PL) quenching yield, [1 − PL(blend)]/PL(pure donor)] × 100%, of the donor photoluminescence for C6PT2C6:F8TCPS, C6PT2C6:F8TIPS and C6PT2C6:F8TIBS blends under various processing conditions.

(150 K for the single crystal, 298 K for GIWAXS). Single crystal X-ray scattering of C6PT2C6 at 298 K confirmed that the volume increase of roughly 5% (2593 Å^3 to 2722 Å^3) is consistent with thermal expansion. It should be noted that all single crystal data were collected at cryogenic temperatures, so we expect thermal expansion to produce small shifts in unit cell parameters relative to the single crystal structures for all the compounds in this study.

Crystallites of C6PT2C6 exhibit preferential (100) orientation in thin films (this lattice plane is rendered in Fig. 1). The conjugated portion of C6PT2C6 is oriented at roughly a 20° angle to the substrate and both sets of alkyl substituents on C6PT2C6 are oriented toward the interfaces of the film with PEDOT and air. The orientational spread (or distribution of the tilt angle) of the crystallites in the film, as measured by the FWHM of the polar angle for the observed reflections, is ∼14°. The FWHM of the (100) peak at a polar angle, χ, of 86° (near $q_{xy} = 0$) gives crystallite correlation length of ∼24 nm.[27] We note that this does not represent the FWHM of highly oriented crystallites, which are in the "missing wedge" of the grazing incidence scattering data. The atomic force micrographs (AFMs) show elongated domains (Fig. SI-1†) where the long direction of the crystallites is the direction of fastest growth, likely the *c* axis of the crystal, along which close π–π interactions are observed. Although the domains are larger than 50 nm in the AFM, the FWHM of the (020) reflection at $q_{xy} = 0.035$ Å^{-1} gives a correlation length ∼30 nm. This difference suggests that the domains in the AFM images are not single crystallites or that cumulative disorder destroys long-range order within them. The observation of such disorder is consequential for organic semiconductors, in which the orbital overlap between molecules is crucial to charge carrier transport.[48]

Ordering of F8TIPS in neat films and BHJs. The acceptor F8TIPS appears to adopt a thin film structure similar to that of

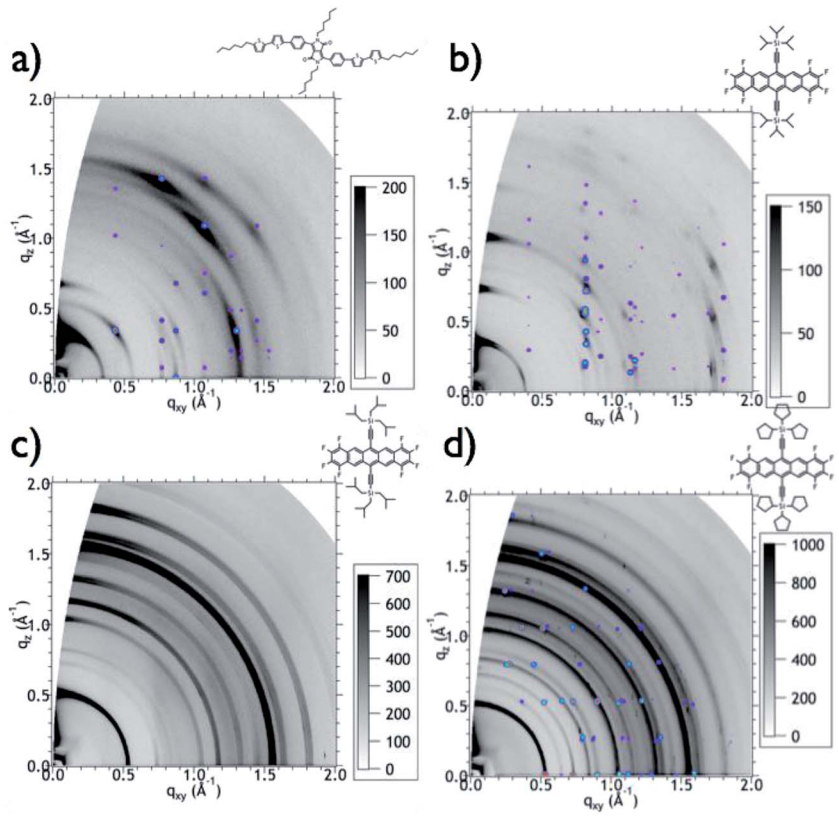

Fig. 5 GIWAXS of neat donor and acceptor films overlayed with peaks from the bulk single crystal structure. (a) C6PT2C6; room temperature unit cell, (b) F8TIPS; bulk single crystal unit cell; (c) F8TIBS; no unit cell determined (d) F8TCPS bulk crystal unit cell adjusted for thermal expansion. Fits for adjusted unit cells can be seen as 1D plots in ESI.†

the bulk single crystal. We observe that all reflections along q_z appear to be split into two peaks with very similar *d*-spacings, and speculate that this results from the presence of a thin film polymorph, although it could also be due to scattering from the film roughness (AFM of a neat film of the F8TIPS acceptor is included in the ESI†). It should be noted that a similar compound, TIPS pentacene, exhibits a thin film polymorph.[36] While this complicates analysis, the packing in the thin film phases is similar enough to what is observed in the single crystal structure to enable us to draw some conclusions. The simulated diffraction pattern obtained from the bulk crystal structure of F8TIPS, with (001) planes oriented parallel to the substrate, is overlaid on the GIWAXS pattern in Fig. 5. It is clear that the (01*l*) family of reflections, which should appear as a series of peaks along $q_{xy} \sim 0.4$, is absent in the experimental data likely from a change in symmetry (*i.e.* the space group). The bulk unit cell of F8TIPS is similar to that of TIPS pentacene, with two salient structural differences: F8TIPS, with $Z = 2$, has *b* axis length almost exactly double that of TIPS pentacene, which has $Z = 1$. It is conceivable that F8TIPS could adopt a TIPS pentacene-like thin film structure in which both molecules in its unit cell are symmetrically equivalent. This would account for the missing family of reflections in a diffraction pattern that is otherwise close to what we would expect of the F8TIPS bulk unit cell. We do observe small shifts in unit cell lengths and angles as a result of thermal expansion, and it is possible that subtle shifts in molecular geometry (*e.g.* distortions of the acene core from planarity) could result in small changes in scattering intensity for the diffraction peaks. As expected from the crystallographic planes containing close co-facial π–π stacking, the film adopts an orientation with [001] along the surface. The tilt angle distribution of this film is about 3°, the lowest of all the films investigated in this work, and many higher-order reflections are apparent. The crystallite correlation length, estimated by the Scherrer analysis on the (001) reflection, is around 80 nm at a polar angle of 86°.

The packing of as-cast blends of F8TIPS with C6PT2C6 shows significant differences from the neat film of either component, although thermal annealing restores the packing found in the single crystal structures of both the donor and acceptor. Our investigations for all donor–acceptor blends in this study focus on a 1 : 1 blend ratio, which yielded the best solar cell performance (see ESI†). The GIWAXS of as-cast F8TIPS/C6PT2C6 blend films shows weaker scattering than neat films, although a large number of peaks are still observable (Fig. 6). However, these reflections do not appear to correspond to any peaks from the bulk cell of the donor or the acceptor. The ordered material in this blend has a crystallite correlation length around 25 nm based on the FWHM of the peak appearing at 0.85 $Å^{-1}$. One notable feature in the GIWAXS is a very prominent peak along q_{xy} corresponding to a *d*-spacing of 3.51 Å, likely indicating in-plane π–π stacking interactions. It is surprising that the as-cast BHJ adopts a structure so different from the crystal structure of either donor or acceptor; GIWAXS of the thermally annealed blend clearly shows (100) oriented C6PT2C6 and (001) oriented F8TIPS, each with crystallite orientation distribution of 7° (Fig. 6; overlay of bulk structure shown in Fig. SI-8†). The donor crystallites have a correlation length around 35 nm, and the acceptor around 27 nm based on the FWHM of the (100) donor peak and the (002) acceptor peak at a polar angle of 86°. These

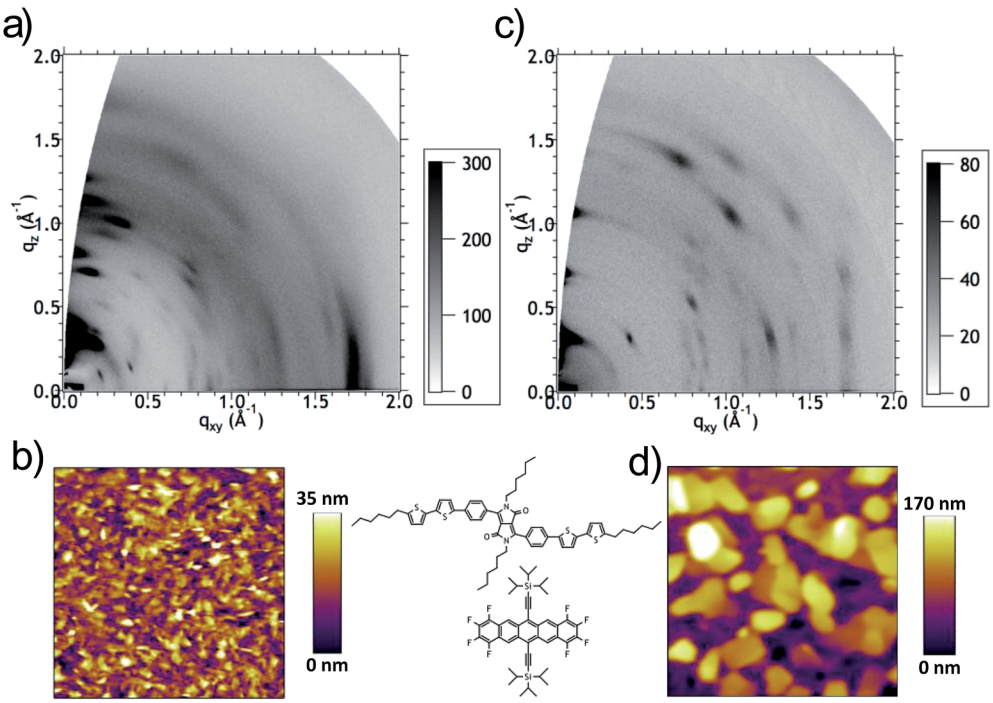

Fig. 6 Morphological data for as-cast and annealed films of F8TIPS : C6PT2C6 (1 : 1 by weight). GIWAXS and AFM topography for as-cast film shown in (a) and (b); GIWAXS and AFM topography for annealed film shown in (c) and (d) (AFM images are 5 × 5 μm).

structural changes are reflected in the UV/Vis of the blend (Fig. 2). In the as-cast film, the acene has a single absorbance band around 335 nm, but after annealing the blend, the intensity of this absorbance decreases significantly and a second band appears around 370 nm. This band is also present in the neat F8TIPS film (Fig. SI-4†) and likely arises from intermolecular interactions between acceptor molecules. AFM images (Fig. 6) show what appear to be small crystallites in as-cast films, and significantly larger aggregates that appear somewhat faceted in annealed films. We note that the AFM of these films probes only the top surface and does not necessarily reflect the structural changes we see in the scattering data from the bulk. Conducting AFM data on these films mainly showed correlation with topography without significant intradomain variation (see ESI†).

The F8TIPS:C6PT2C6 BHJs are relatively inefficient (<0.1% PCE) due to their very low J_{sc} (data summarized in Fig. 3 and Table 2). Based on AFM data alone, we might predict a decrease in J_{sc} upon annealing the blend, because domains larger than the a typical exciton diffusion length (~5 to 10 nm for the donor C6PT2C6) should result in more recombination and less effective charge transfer.[49] However, the GIWAXS data correlates to the solar cell characteristics: we observe that J_{sc} doubles upon annealing, suggesting that the structural change improves charge generation with only a small increase in the FF. The electron and hole mobilities from space charge current limited diodes show an apparent decrease upon annealing leading to both having a similar low value.

Ordering of F8TIBS in neat films and BHJs. F8TIBS differs chemically from F8TIPS by only a methylene unit between the silicon atoms and each isopropyl substituent; it is the only compound for which we could not obtain a refinable crystal structure. Unlike the other acceptors in the series, the AFM for F8TIBS (Fig. SI-1†) indicates that it forms smooth, continuous films, such as those we might expect from an amorphous material. The neat F8TIBS films show a sharp absorbance around 330 nm, unlike the other acceptor films, in which this band is significantly broadened with a "shoulder" around 360–370 nm (Fig. SI-4†). We do not observe discrete spots from this compound in the GIWAXS, but we do see scattering in arcs, which indicate aggregation between molecules in a film with orientation distribution around 15° (Fig. 5). (The appearance of rings results from arcs that overlap.) Among the rings, two progressions of *d*-spacings are observed, corresponding to 12.0 Å and 7.6 Å, with apparent correlation lengths of 65 and 42 nm, respectively, based on the FWHM with a polar angle of 86°.

F8TIBS crystallizes with highly oriented crystallites in BHJs despite being poorly textured in thin films. Upon blending F8TIBS with C6PT2C6, we observe peaks due to crystalline C6PT2C6, but no longer see scattering rings corresponding to the acceptor. Instead we observe discrete reflections, mostly near the q_z axis, with a preferred texture that we attribute to the acceptor (Fig. 7). The orientational distribution of the F8TIBS crystallites is around 12°, with average thickness only about 24 nm. It is notable that the intense overlapping arcs observed off-axis in the neat acceptor film are not discernible in the blend film. It seems that the acceptor crystallizes in the blend with long-range order along q_z. Additionally, an intense peak has appeared along q_{xy}, corresponding to a *d*-spacing of 3.46 Å. This peak can be attributed to π–π stacking interactions, although it is unclear whether F8TIBS is associating with a donor molecule or with another F8TIBS molecule. C6PT2C6 crystallites

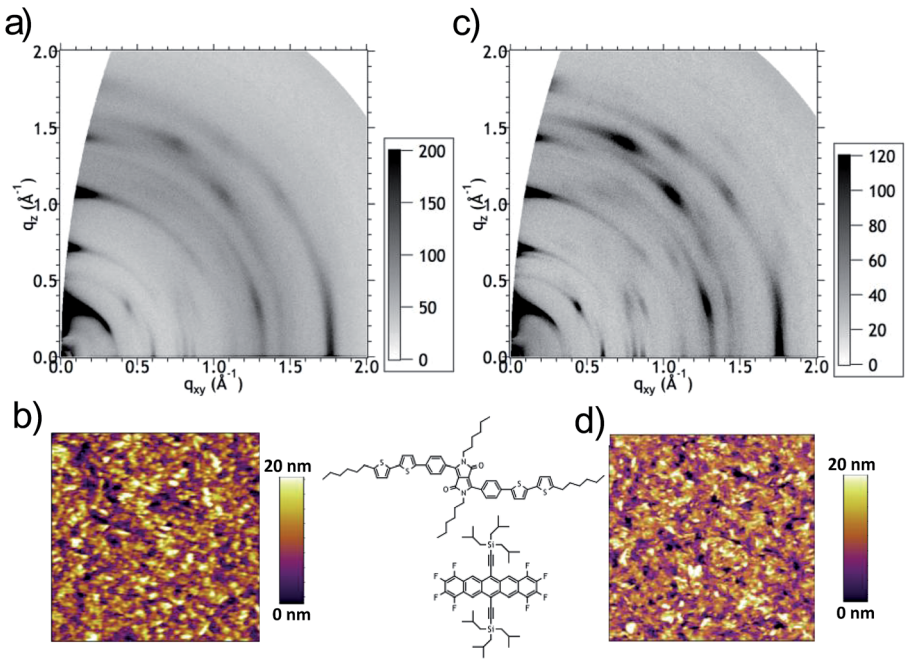

Fig. 7 Morphological data for thin films of F8TIBS : C6PT2C6 (1 : 1 by weight). GIWAXS and AFM topography for as-cast film shown in (a) and (b); GIWAXS and AFM topography for annealed film shown in (c) and (d) (AFM images are 5 × 5 μm).

(thickness of at least 50 nm by the FWHM of the (100) reflection at a polar angle of 86°) may nucleate the growth of F8TIBS, templating a particular texture of F8TIBS crystallites. This hypothesis would explain the more highly oriented F8TIBS film in the blend relative to the F8TIBS neat film because C6PT2C6 exhibits a strongly preferred orientation in nearly all films, an 11° orientation distribution comparable to its neat film. Upon annealing the film, we observe the appearance of high order reflections corresponding to acceptor F8TIBS along q_z (Fig. 7). No clear indication of crystallinity is observable by the topography in AFM images that indicates a relatively smooth film with no immediately apparent crystalline features (Fig. 7).

While the morphology of the F8TIBS films is the smoothest of the series we investigated, and is most similar in appearance to the topography of high-performance BHJs, the short-circuit current density is the lowest of the series (Fig. 3 and Table 2). The PL quenching yield is highest for this blend in the series in agreement with the small domain sizes (Fig. 4). The electron mobility of the blend is also relatively low in comparison to the rest of the series. Even with clearly evident π–π stacking interactions in the blend, and even with domain sizes approximately on the order of what is considered optimal for a bulk heterojunction, it appears that the lack of 3-D crystalline ordering within F8TIBS (we only observe higher order reflections along q_z in the blend) leads to low mobility, impeding charge extraction.

Ordering of F8TCPS in neat films and BHJs. F8TCPS leads to highest performance in solar cells with C6PT2C6. GIWAXS of as-cast films indicates a weak preference for (110) orientation, with a 22° spread of orientations, and many scattering rings that overlap significantly (Fig. 5). The GIWAXS data is fit well by the bulk structure with small adjustments for thermal expansion, as shown by the simulated diffraction pattern overlay and the powder figure (Fig. SI-9†). The relatively wide distribution of orientations for this compound is expected because several crystal faces (110 and −110, for example) should have similar surface energies because they comprise a mixture of alkyl groups and acene cores. AFM topography of the neat acceptor film (Fig. SI-1†) appears similar to that for F8TIBS, exhibiting a fairly continuous film, but some aggregates that are faceted are also present in the film.

In BHJ films, F8TCPS is disordered initially, but crystallizes after thermal processing. In the as-cast F8TCPS blend, though, the donor is also disordered, and no clear donor peaks are present in the GIWAXS data (Fig. 8). (Although a peak appears where we expect the donor (331) reflection, we do not observe other reflections for which we predict higher scattering intensity.) Thermal annealing for this blend leads to ordering of both components, producing discrete reflections with the typical (100) texture, 10° tilt angle distribution and an apparent crystallite thickness of 52 nm for C6PT2C6, based on the (100) reflection at a polar angle of 86° (Fig. 8). For F8TCPS, we observe (110) orientation with 8° spread and 38 nm crystallite thickness.

The F8TCPS:C6PT2C6 BHJs have low efficiency (PCE < 1% PCE) due to their very low J_{sc} (data summarized in Fig. 3 and Table 2), but do improve upon thermal annealing. Interestingly the quenching yield decreases with annealing from ~60% to 40% indicating that the improved structural order of the acceptor improves the PCE mainly through more efficient charge extraction (higher FF).

Comparison of acceptors

Our results demonstrate that the internal molecular packing of the F8TCPS crystallites is the key to its optoelectronic

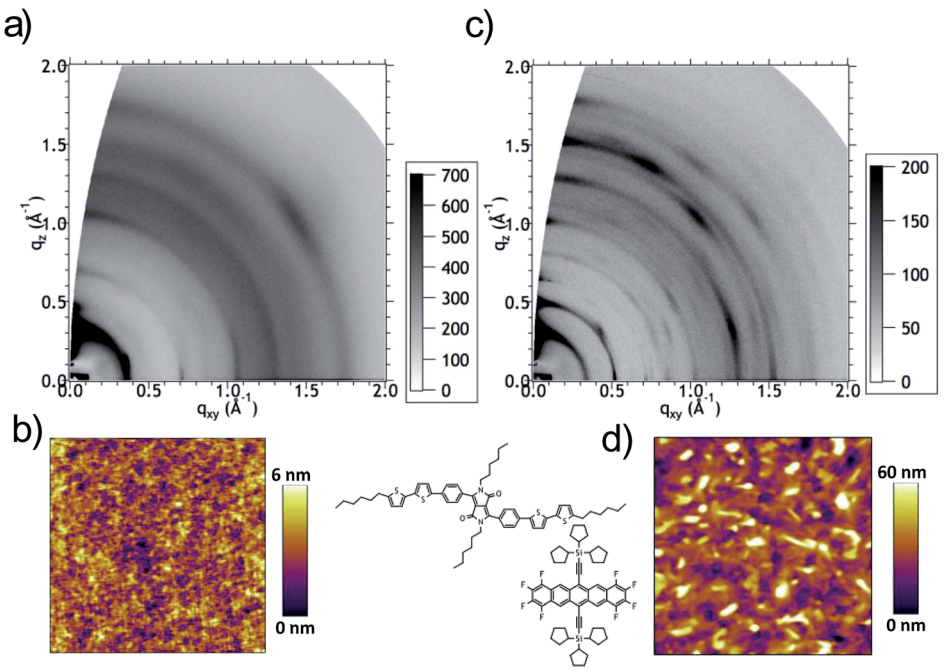

Fig. 8 Morphological data for thin films of F8TCPS : C6PT2C6 (1 : 1 by weight). GIWAXS and AFM topography for as-cast film shown in (a) and (b); GIWAXS and AFM topography for annealed film shown in (c) and (d) (AFM images are 5 × 5 μm).

performance. Of all blends studied in this series, those containing F8TCPS have the highest J_{sc}, including the as-cast blend in which the acceptor is less ordered relative to the annealed film (Fig. 3; Table 2). This observation contrasts with the results for the F8TIBS blend, in which poorly ordered acceptor phases lead to low J_{sc}. An important difference in this case is that the donor domains are also disordered. Of the F8TCPS blends, the fill factor is highest for the thermally annealed films, in which the donor and acceptor are both crystalline. Thermally annealed F8TCPS blend films have hole mobilities twice as high and electron mobilities four times as high as untreated blends. Thus we find that, as in the case of P3HT as a donor, the "sandwich herringbone" packing shown by F8TCPS produces the best performance with molecular donors.[25] While the power conversion efficiencies are low in both cases, the fact that F8TCPS is the best acceptor for both a semicrystalline polymer and a crystalline molecular donor support the conclusion that the molecular packing in the acceptor is the origin.

The short circuit current is low for all of the blends studied here, but the PL quenching yield is high. Therefore photophysical properties of acceptors are also as important as molecular packing. For example, TIPS-pentacene is known to undergo singlet fission and the resulting triplet state may have too low of an energy to drive the electron transfer in the BHJs studied here with high open circuit voltage.[50] Our results here do, however, indicate that the sandwich herringbone packing allows the charges that are generated to be extracted at the contacts.

Conclusions

We have studied the morphology and crystallization of pentacene-based acceptors in BHJs with a diketopyrrolopyrrole-based small molecule donor. In these BHJs, both the donor and acceptor form crystalline domains. In contrast, PCBM and other fullerene acceptors, which perform well in BHJ solar cells, are disordered. Because fullerenes have a relatively spherical shape their electronic coupling is less sensitive to molecular orientation. Our observations in this study indicate that for nearly planar small molecule non-fullerene acceptors, amorphous domains may not be advantageous for BHJs. We observe consistently low J_{sc} for blends in which a pentacene-based acceptor is disordered. Additionally, the fill factor appears to be sensitive to ordering within both components, and is highest for cases in which donor and acceptor are both ordered. The "sandwich herringbone" packing shown by F8TCPS produces the best performance with molecular donors and has the same trend as for P3HT cells, suggesting that this is a preferable packing motif for these molecular acceptors.

We find significant changes in molecular ordering in BHJs relatively to neat films. In as-cast BHJ films, F8TIPS exhibits a completely unforeseen structure because it is sterically unencumbered relative to the other acceptors and can associate very closely with the donor. However, after thermal annealing both the donor and acceptor revert to their bulk crystal structures, demonstrating the important role of processing in establishing molecular order. F8TIBS, the second smallest, loses long-range order when blended with donor, except in the out-of-plane direction, and we do not see changes upon annealing. This observation, along with our lack of success in growing single crystals, indicates that nucleation of crystallites of F8TIBS is difficult and that it is an unsuitable small molecule acceptor. F8TCPS, which is sterically encumbered, is disordered upon initial casting of a blend film, but becomes ordered upon thermal annealing. This property may allow formation of nanoscale domains and a means to improve the crystalline ordering critical for increasing the power conversion efficiency.

Structural characterization of organic semiconductor molecules within a biphasic BHJ is complicated due to the disorder present in thin films, but GIWAXS provides valuable insight into molecular packing and ordering within the film. Single crystal structures are helpful in data analysis, but polymorphism in thin films can lead to unit cells that are not equivalent to those observed for bulk crystals complicating the analysis. In cases such as as-cast BHJs of F8TIPS, where a new structure is present that may contain one or both compounds present in the blend, it is very difficult to extract the molecular arrangement due to the relatively low number of diffraction peaks and question of composition. In such cases, molecular spectroscopies, *e.g.* spectroscopic ellipsometry or polarized infrared spectroscopy, can provide insight into the molecular order.[51,52]

Acknowledgements

JBS was supported by a DOE Graduate Fellowship and by the Center for Energy Efficient Materials, an Energy Frontier Research Center funded by the U.S. Department of Energy, Office of Science, Office of Basic Energy Sciences under Award Number DE-SC0001009. CK, SC, and TQN were partially supported by the NSF SOLAR program (DMR 1035480). JEA and BP were supported by the NSF SOLAR program (DMR 1035257). The MRL Shared Experimental Facilities are supported by the MRSEC Program of the NSF under Award no. DMR 1121053; a member of the NSF-funded Materials Research Facilities Network (http://www.mrfn.org). Portions of this research were carried out at the Stanford Synchrotron Radiation Lightsource, a directorate of SLAC National Accelerator Laboratory and an Office of Science User Facility operated for the U.S. Department of Energy Office of Science by Stanford University. We gratefully thank Dag Brieby for the SimDiffraction software.

Notes and references

1 G. Yu, J. Gao, J. C. Hummelen, F. Wudl and A. J. Heeger, *Science*, 1995, **270**, 1789–1791.
2 G. Li, R. Zhu and Y. Yang, *Nat. Photonics*, 2012, **6**, 153–161.
3 Z. He, C. Zhong, S. Su, M. Xu, H. Wu and Y. Cao, *Nat. Photonics*, 2012, **6**, 591–595.
4 J. Zhou, X. Wan, Y. Liu, Y. Zuo, Z. Li, G. He, G. Long, W. Ni, C. Li, X. Su and Y. Chen, *J. Am. Chem. Soc.*, 2012, **134**, 16345–16351.
5 A. K. K. Kyaw, D. H. Wang, D. Wynands, J. Zhang, T.-Q. Nguyen, G. C. Bazan and A. J. Heeger, *Nano Lett.*, 2013, **13**, 3796–3801.

6 Y. Lin and X. Zhan, *Mater. Horiz.*, 2014, **1**, 470.
7 A. F. Eftaiha, J.-P. Sun, I. G. Hill and G. C. Welch, *J. Mater. Chem. A*, 2014, **2**, 1201.
8 M. T. Lloyd, J. E. Anthony and G. G. Malliaras, *Mater. Today*, 2007, **10**, 34–41.
9 J. Roncali, P. Leriche and P. Blanchard, *Adv. Mater.*, 2014, **26**, 3821–3838.
10 P. M. Beaujuge and J. M. J. Fréchet, *J. Am. Chem. Soc.*, 2011, **133**, 20009–20029.
11 B. Verreet, B. P. Rand, D. Cheyns, A. Hadipour, T. Aernouts, P. Heremans, A. Medina, C. G. Claessens and T. Torres, *Adv. Energy Mater.*, 2011, **1**, 565–568.
12 G. Chen, H. Sasabe, Z. Wang, X.-F. Wang, Z. Hong, Y. Yang and J. Kido, *Adv. Mater.*, 2012, **24**, 2768–2773.
13 J. J.-A. Chen, T. L. Chen, B. Kim, D. A. Poulsen, J. L. Mynar, J. M. J. Fréchet and B. Ma, *ACS Appl. Mater. Interfaces*, 2010, **2**, 2679–2686.
14 P. Sonar, J. P. F. Lim and K. L. Chan, *Energy Environ. Sci.*, 2011, **4**, 1558–1574.
15 J. T. Bloking, X. Han, A. T. Higgs, J. P. Kastrop, L. Pandey, J. E. Norton, C. Risko, C. E. Chen, J.-L. Brédas, M. D. McGehee and A. Sellinger, *Chem. Mater.*, 2011, **23**, 5484–5490.
16 T. V. Pho, F. M. Toma, M. L. Chabinyc and F. Wudl, *Angew. Chem., Int. Ed.*, 2013, **52**, 1446–1451.
17 X. Zhang, Z. Lu, L. Ye, C. Zhan, J. Hou, S. Zhang, B. Jiang, Y. Zhao, J. Huang, S. Zhang, Y. Liu, Q. Shi, Y. Liu and J. Yao, *Adv. Mater.*, 2013, **25**, 5791–5797.
18 T. Earmme, Y.-J. Hwang, N. M. Murari, S. Subramaniyan and S. A. Jenekhe, *J. Am. Chem. Soc.*, 2013, **135**, 14960–14963.
19 A. Sharenko, C. M. Proctor, T. S. van der Poll, Z. B. Henson, T.-Q. Nguyen and G. C. Bazan, *Adv. Mater.*, 2013, **25**, 4403–4406.
20 J. D. Douglas, M. S. Chen, J. R. Niskala, O. P. Lee, A. T. Yiu, E. P. Young and J. M. J. Fréchet, *Adv. Mater.*, 2014, **26**, 4313–4319.
21 P. E. Shaw, P. Wolfer, B. Langley, P. L. Burn and P. Meredith, *J. Phys. Chem. C*, 2014, **118**, 13460–13466.
22 J. E. Anthony, *Chem. Mater.*, 2011, **23**, 583–590.
23 M. A. Brady, G. M. Su and M. L. Chabinyc, *Soft Matter*, 2011, **7**, 11065–11077.
24 A. J. Ferguson, J. L. Blackburn and N. Kopidakis, *Mater. Lett.*, 2013, **90**, 115–125.
25 Y.-F. Lim, Y. Shu, S. R. Parkin, J. E. Anthony and G. G. Malliaras, *J. Mater. Chem.*, 2009, **19**, 3049.
26 G. R. Desiraju and A. Gavezzotti, *Acta Crystallogr., Sect. B: Struct. Sci.*, 1989, **45**, 473–482.
27 J. Rivnay, R. Noriega, J. E. Northrup, R. J. Kline, M. F. Toney and A. Salleo, *Phys. Rev. B: Condens. Matter Mater. Phys.*, 2011, **83**, 121306(R).
28 J. E. Anthony, D. L. Eaton and S. R. Parkin, *Org. Lett.*, 2002, **4**, 15–18.
29 B. Purushothaman, M. Bruzek, S. R. Parkin, A.-F. Miller and J. E. Anthony, *Angew. Chem., Int. Ed.*, 2011, **50**, 6932–6932.
30 M. L. Tang and Z. Bao, *Chem. Mater.*, 2011, **23**, 446–455.
31 C. Kim, J. Liu, J. Lin, A. B. Tamayo, B. Walker, G. Wu and T.-Q. Nguyen, *Chem. Mater.*, 2012, **24**, 1699–1709.
32 B. Walker, J. Liu, C. Kim, G. C. Welch, J. K. Park, J. Lin, P. Zalar, C. M. Proctor, J. H. Seo, G. C. Bazan and T.-Q. Nguyen, *Energy Environ. Sci.*, 2013, **6**, 952.
33 K. S. Yook, B. D. Chin, J. Y. Lee, B. E. Lassiter and S. R. Forrest, *Appl. Phys. Lett.*, 2011, **99**, 043308.
34 Y. Sun, G. C. Welch, W. L. Leong, C. J. Takacs, G. C. Bazan and A. J. Heeger, *Nat. Mater.*, 2012, **11**, 44–48.
35 R. A. Laudise, C. Kloc, P. G. Simpkins and T. Siegrist, *J. Cryst. Growth*, 1998, **187**, 449–454.
36 S. C. B. Mannsfeld, M. L. Tang and Z. Bao, *Adv. Mater.*, 2011, **23**, 127–131.
37 J. Zhang, H. Geng, T. S. Virk, Y. Zhao, J. Tan, C. Di, W. Xu, K. Singh, W. Hu, Z. Shuai, Y. Liu and D. Zhu, *Adv. Mater.*, 2012, **24**, 2603–2607.
38 K. Vasseur, B. P. Rand, D. Cheyns, K. Temst, L. Froyen and P. Heremans, *J. Phys. Chem. Lett.*, 2012, **3**, 2395–2400.
39 A. Viterisi, N. F. Montcada, C. V. Kumar, F. Gispert-Guirado, E. Martin, E. Escudero and E. Palomares, *J. Mater. Chem. A*, 2014, **2**, 3536.
40 C. R. Swartz, S. R. Parkin, J. E. Bullock, J. E. Anthony, A. C. Mayer and G. G. Malliaras, *Org. Lett.*, 2005, **7**, 3163–3166.
41 J. E. Anthony, J. S. Brooks, D. L. Eaton and S. R. Parkin, *J. Am. Chem. Soc.*, 2001, **123**, 9482–9483.
42 Y. Shu, Y.-F. Lim, Z. Li, B. Purushothaman, R. Hallani, J. E. Kim, S. R. Parkin, G. G. Malliaras and J. E. Anthony, *Chem. Sci.*, 2011, **2**, 363.
43 M. Tantiwiwat, Physics, in *Structure–function–property relationships in solution-processed diketopyrrolopyrrole-based materials*, University of California, Santa Barbara, Santa Barbara, Calif., 2011.
44 A. Armin, I. Kassal, P. E. Shaw, M. Hambsch, M. Stolterfoht, D. M. Lyons, J. Li, Z. Shi, P. L. Burn and P. Meredith, *J. Am. Chem. Soc.*, 2014, **136**, 11465–11472.
45 J. D. A. Lin, J. Liu, C. Kim, A. B. Tamayo, C. M. Proctor and T.-Q. Nguyen, *RSC Adv.*, 2014, **4**, 14101.
46 A. D. Platt, J. Day, S. Subramanian, J. E. Anthony and O. Ostroverkhova, *J. Phys. Chem. C*, 2009, **113**, 14006–14014.
47 D. W. Breiby, O. Bunk, J. W. Andreasen, H. T. Lemke and M. M. Nielsen, *J. Appl. Crystallogr.*, 2008, **41**, 262–271.
48 J. Rivnay, R. Noriega, J. E. Northrup, R. J. Kline, M. F. Toney and A. Salleo, *Phys. Rev. B: Condens. Matter Mater. Phys.*, 2011, **83**, 121306.
49 O. V. Mikhnenko, J. Lin, Y. Shu, J. E. Anthony, P. W. M. Blom, T.-Q. Nguyen and M. A. Loi, *Phys. Chem. Chem. Phys.*, 2012, **14**, 14196.
50 C. Ramanan, A. L. Smeigh, J. E. Anthony, T. J. Marks and M. R. Wasielewski, *J. Am. Chem. Soc.*, 2012, **134**, 386–397.
51 D. M. DeLongchamp, R. J. Kline, D. A. Fischer, L. J. Richter and M. F. Toney, *Adv. Mater.*, 2011, **23**, 319–337.
52 W. Chen, M. P. Nikiforov and S. B. Darling, *Energy Environ. Sci.*, 2012, **5**, 8045.

